Modulation of Prosthetic Ankle Plantarflexion Through Direct Myoelectric Control of a Subject-Optimized Neuromuscular Model

Tony Shu, Christopher Shallal, Ethan Chun, Aashini Shah, Angel Bu, Daniel Levine, Seong Ho Yeon, Matthew Carney, Hyungeun Song, Tsung-Han Hsieh, and Hugh M. Herr

Abstract— **The ideal neuroprosthetic control paradigm minimizes disparities in dynamic performance and subjective embodiment between artificial and intact physiology. In this letter, we address the former by introducing the Activation Mapping paradigm, a cascaded optimization procedure that enables a subject with unilateral transtibial amputation to neurally modulate the torque developed during prosthetic ankle plantarflexion. Specifically, in the first stage, the optimization procedure develops a digital locomotor clone that recovers symmetric gait dynamics for the hypothetical subject prior to amputation. In the second stage, the resultant ankle torque-angle trajectory serves as a reference to optimize over the morphological parameters of a neuromuscular ankle model. The optimized model contains a single agonist-antagonist muscle pair driven by a recording of the subject's within-socket walking electromyograms that reproduces the reference ankle dynamics. In this manner, the subject's natural residual muscular activations are mapped to their idealized gait dynamics to form a one degree-of-freedom neuromuscular ankle controller. The subsequent implementation of the activation map on a powered ankle prosthesis enables the subject to not only generate physiological ankle dynamics to increase their self-selected walking speed from 1.22 m/s to 1.33 m/s, but also to volitionally perform bilaterally symmetric standing calf raises while balancing for at least 2.0 seconds.**

I. INTRODUCTION

The dynamics of human walking are well-characterized, and the roles of individual lower-extremity joints during the gait cycle are understood in relation to their functional and clinical significance. Of particular importance is the role of the ankle joint in the sagittal plane of movement. The ankle performs net work against the environment with a typical peak rate of $3.5 W kg^{-1}$ during preferred level-ground walking speeds [1]. This effort has been alternately hypothesized to redirect the body's center of mass [2], reduce energetic losses at the leading leg during touch down [3], and efficiently propel the trailing leg into its swing phase [4]. Correspondingly, loss of the joint from amputation commonly results in detrimental health outcomes such as increased metabolic cost of transport [5][6] and patellofemoral osteoarthritis in the contralateral leg [7].

Despite several mechanical innovations and a slew of novel environmental sensing modalities [8][9], current powered ankle prostheses have not been shown to achieve direct volitional controllability to the same degree as intact physiology [10]. However, one class of physiological lower-extremity signals, surface electromyography (sEMG), has demonstrated utility for control of both powered ankle prostheses and powered ankle orthoses [11][12][13][14][15][16]. Continued investigation is warranted to determine if the proper combination of sEMG processing and controller design can further ameliorate this disparity.

In this study, we hypothesize that a controller-prosthesis system which can generate physiologically-inspired ankle joint dynamics from untrained, within-socket residual muscle activity restores the ability to actively modulate plantarflexion torque for the purposes of level-ground speed adaptation and tiptoe balancing. To test this hypothesis, we first extract a transtibial amputee subject's idealized ankle dynamics by optimizing the gait of a digital locomotor clone driven by spinal reflexive loops. Next, the subject is asked to walk with their prescribed passive prosthesis while within-socket residual lateral gastrocnemius (GAS) and tibialis anterior (TA) sEMG signals are recorded. In a subsequent optimization, the recorded sEMG signals are used to activate a neuromuscular agonist-antagonist model that kinematically-tracks the idealized ankle angle trajectory. The optimization determines the morphological parameters of the model that minimize the RMS error between recorded sEMG-determined and idealized ankle torque trajectories, thus mapping recorded sEMG to idealized dynamics. This activation map (AM) controller is implemented on a powered ankle prosthesis, and the subject is asked to walk on a split-belt treadmill, walk over level-ground, and perform calf raises while modulating their muscle activity to determine plantarflexion torque. The efficacy of the AM control paradigm is assessed through analysis of measured ankle dynamics and ground reaction forces.

II. BACKGROUND

A. sEMG Control of Powered Ankle Prostheses

Surface EMG signals have been explored as a limited control method in various applications of powered ankle prostheses [11][12][13][16][17]. In 2005, Au *et al.* demonstrated impedance-based control of a powered ankle in free

Tony Shu, Daniel Levine, Seong Ho Yeon, Matthew Carney, Tsung-Han Hsieh, and Hugh Herr are with the Media Lab, MIT, Cambridge 02142, USA (email: tonyshu@mit.edu; dvlevine@mit.edu; syeon@mit.edu; mcarney@mit.edu; thhsieh@mit.edu; hherr@mit.edu)

Christopher Shallal and Hyungeun Song are with Harvard-MIT Program in Health Sciences and Technology, MIT, Cambridge 02142, USA (email: cshallal@mit.edu; hngnsong@mit.edu)

Ethan Chun is with the Department of Electrical Engineering and Computer Science, MIT, Cambridge 02142, USA (email: elchun@mit.edu)

Aashini Shah and Angel Bu are with the Department of Mechanical Engineering, MIT, Cambridge 02142, USA (email: aashah28@mit.edu; angelbu@mit.edu)

space using a bilinear muscle model [11]. Electrodes were attached to the residual limb without a socket, and the subject was able to track a desired plantarflexion trajectory with visual feedback. In 2008, Au *et al.* used sEMG to determine transitions between level-ground and stair-descent impedance-based finite state machines [12]. Wang *et al.* utilized sEMG from a custom socket liner with embedded electrodes to modulate the gain of a positive force feedback control loop to command powered plantarflexion torque [13]. Huang *et al.* demonstrated continuous modulation of plantarflexion torque from proportional sEMG [16]. Their work utilized repeatedly hand-tuned controller gains and relied on providing subjects a visual reference for desired plantarflexion torque. Clites *et al.* demonstrated active sEMG control of prosthetic ankle and subtalar positions in free space using hand-tuned controller gains, but did not use sEMG to determine torque during stance phases [17].

Additionally, the techniques used in these previous studies to measure sEMG are generally incompatible with the sustained use of prescription prosthetic sockets due to bulky physical sensors, pre-amplifiers, and wires that painfully indent the skin [18]. However, a recent advance in flexible, dry electrode design is compatible for use inside prescription sockets and liners without modification [19][20].

B. Spinal Reflexive Architectures

In contrast to the volitional nature of using measured sEMG for control of joint dynamics, much work has been done to study central nervous system (CNS) spinal reflexive control loops that use signals such as muscle force, length, and velocity to yield organismal biomechanics. The Geyer-Herr model was the first to demonstrate principles of bipedal locomotion in this way [21]. Subsequently, Song *et al.* created a digital locomotor clone with 11 Hill-type muscles per leg and 10 spinal reflex modules to demonstrate ramp ascent/descent, navigation of uneven terrain, and turning [22]. This was achieved by using the nonlinear covariance matrix adaptation evolution strategy (CMA-ES) [23] to tune 82 control parameters while referencing a 3-tier cascaded cost function that prioritizes not falling, steady step-to-step gait, and target walking velocity and minimal metabolic cost of transport, in that order. The joint dynamics generated by Song *et al.'s* digital locomotor clone match known values from clinical studies, yet can be determined purely through simulation.

In parallel, prosthesis controllers based on CNS reflexive pathways have previously demonstrated the ability to provide terrain-dependent work loop adaptations [24][25][26]. Some of these controllers implemented neuromuscular models optimized to generate an idealized muscle activation or torque trajectory using observations of height- and weight-matched non-amputee reference subjects. While these approaches produce reasonable torque-angle phase portraits during stance, they are not actively informed by sEMG measured from the residual limb and are thus unable to achieve volitional behaviors. The user of such reflexive controllers "rides" the device, as opposed to driving it.

Though individually substantial, none of these studies used sEMG to continuously generate ankle torque in an intuitive manner through direct stimulation of a neuromuscular model during powered plantarflexion.

III. ACTIVATION MAPPING PARADIGM

The AM paradigm seeks to procedurally map measured within-socket sEMG to physiologically-inspired ankle dynamics in a manner that provides intuitive control over prosthetic ankle torque. Because unilateral transtibial amputees do not possess bilateral symmetry, a digital locomotor clone is used to generate symmetric gait dynamics. This technique supplants previous approaches using roughly-matched human subjects for reference dynamics because the digital locomotor clone can be scaled exactly in a fully observable simulation environment [24][25]. Subsequent use of measured within-socket sEMG signals that incorporate nonlinear ground impact and skin impedance dynamics determine the parameters of a neuromuscular controller, creating a map from achievable sEMG patterns to desired ankle dynamics and potentially reducing uncertainty during online control.

A. Subject Recruitment

A single subject (44 years old, 1.65 m, 64 kg, Caucasian, female) with unilateral left-side transtibial amputation was recruited. The subject's amputation was performed under the Agonist-antagonist Myoneural Interface (AMI) surgical paradigm, forming two dynamically coupled agonist-antagonist muscle pairs—tibialis anterior (TA) paired with lateral gastrocnemius (GAS), and tibialis posterior (TP) paired with peroneous longus (PL)—within the residuum [27]. In this way, the AMI paradigm is hypothesized to provide a greater degree of neuromuscular control through the mechanism of mechanoneural transduction [17]. The subject provided written informed consent through MIT COUHES protocol #1609692618.

B. sEMG Collection and Processing

Flexible polyimide electrodes were used to collect within-socket sEMG signals under the subject's unmodified prosthetic liner. [19][20]. After palpation, four total electrodes were redundantly placed superior to the GAS and TA muscles and fixed in place with hydrogel bandages. The electrode combination that minimized cross-talk was selected to compute GAS and TA activations. Fig. 1A demonstrates muscle locations and electrode placements.

A custom embedded sEMG processor sampled the four data channels at a frequency of 1 kHz [20], [28]. The recently developed cumulative histogram filter (CHF) conditioned raw sEMG into an estimate of muscle activity [29][30][31]. Rectified raw sEMG signals were first band-pass filtered with a pass-band of 20-400 Hz. To mitigate mechanical impact artifacts, a 100 ms window of the band-passed sEMG signals was sorted by amplitude in a CHF with lower bound of 0.1 and upper bound of 0.7 [31]. The RMS power of the filtered sEMG signal of each muscle was used to calculate activation after normalizing by maximum voluntary contraction (MVC).

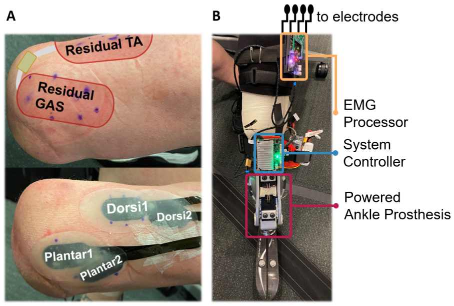

Fig. 1. Neuroprosthesis experimental setup. (A) Locations of palpated AMI muscles and corresponding redundant electrode coverage. (B) Physical layout of computational and mechatronic components.

C. Stage One: Optimization of Reflexive Gait Dynamics

In stage one, Song *et al.*'s digital motor clone is used to generate a reference gait [22]. The digital locomotor clone was scaled to the subject's intact body segment measurements estimated from motion capture data *(Vicon Motion Systems Ltd., Oxford, UK)*. Dimensions of the feet, shanks, thighs, and trunk were scaled to motion marker calibration data taken from corresponding bony anatomical landmarks. Local centers of gravity for each model segment in the sagittal plane were estimated by interpolating from data provided by Dempster and Gaughran [32]. The segments' masses and inertia matrices were determined by scaling an OpenSim `gait2394simbody` model to the subject's dimensions [33][34]. Similarly, each modeled muscle's maximum isometric force, optimal fiber length, and tendon slack length were taken from the scaled OpenSim model. Other muscle parameters and neural transmission delays were assumed common to most individuals and remained unaltered. Fig. 2A demonstrates this scaling procedure.

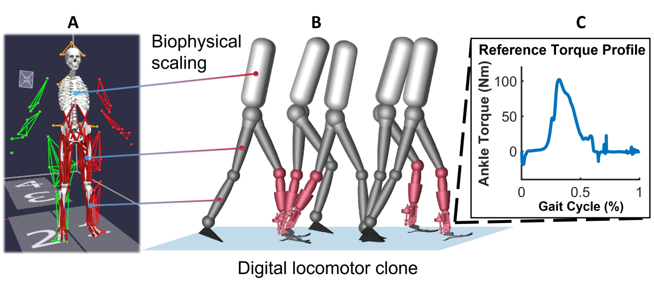

Fig. 2. Stage One: Gait Optimization. (A) Subject measurements are estimated with motion capture data and used to scale (B) a digital locomotor clone. (C) Resultant ankle torque-angle trajectories for one step are obtained after optimizing the digital locomotor clone to walk stably.

The scaled digital locomotor clone was optimized using CMA-ES to walk on level-ground at 1.2 m/s by minimizing Song *et al.*'s 3-tier cost function [22]. In addition to the 82 control parameters that determine the reflexive neural excitation gains, 21 morphological parameters belonging to the model's gastrocnemius, soleus, and tibialis anterior muscles were included in the search space: maximum force, optimal fascicle length, maximum fascicle velocity, tendon slack length, maximum lever arm length, minimum lever arm length, and reference lever arm angle for all three muscles. A single CMA-ES run comprised 400 iterations with each parallelized iteration consisting of 16 digital locomotor clones walking for 15 simulated seconds. Three runs were performed, and the parameter set with the lowest cost was retained. A single run required approximately 30 hours on an AMD Ryzen$^{\text{TM}}$ 3950X CPU. A reference ankle torque-angle trajectory for a single step, partially represented in Fig. 2C, was generated by averaging over the last six steps taken by the optimized digital locomotor clone's left ankle.

D. Stage Two: Optimization of Plantarflexor Morphological Parameters

In stage two, the parameters of a virtual plantarflexor are found that, when paired with the unaltered TA from stage one, best map the subject's own sEMG signals to the reference ankle torque trajectory. This virtual agonist-antagonist pair forms the AM controller. Because the digital locomotor clone's ankle possesses two plantarflexors, it does not readily translate to control of a powered prosthetic ankle when the subject has only one sEMG signal for plantarflexion. Furthermore, it is unknown if the clone's reflexively-generated activation pattern is reachable by the subject. Thus, stage two: a) optimizes a *single* replacement plantarflexor muscle to replace the two in the digital locomotor clone, and b) injects the subject's own measured within-socket sEMG to determine plantarflexor and dorsiflexor activations.

First, the subject was asked to walk on a treadmill *(Bertec Corporation, Columbus, USA)* at 1.2 m/s for two minutes with their passive prosthetic ankle, as seen in Fig. 3A. sEMG signals were recorded from their residual GAS and TA muscles and averaged over 25 steps. These average sEMG trajectories were normalized by the 95th percentile amplitude measured to produce average muscle activation.

The subject's average TA activation trajectory was used to activate the optimized TA muscle from stage one while their average GAS activation trajectory was used to activate the plantarflexor muscle to be optimized, as seen in Fig. 3B. These virtual muscles generated a torque trajectory as the ankle was made to kinematically track the stage one reference angle trajectory. Because of the relative importance of the plantarflexor muscle during stance, only its morphological parameters were optimized while those of the TA remained unaltered. The CMA-ES algorithm was again utilized to optimize over 10 morphological parameters of the replacement plantarflexor to yield the optimal parameter set M^* according to

$$M^* = \min_M \frac{\sum_{t=0}^{n-1} (\tau_M(t) - \tau_{ref}(t))^2}{\sum_{t=0}^{n-1} (\tau_{ref}(t) - \bar{\tau}_{ref})^2} \tag{1}$$

where τ_M is the resultant torque generated from plantarflexor morphological paramater set M, τ_{ref} is the reference torque, and n is the duration from heel strike to toe off in milliseconds. For stage two, the CMA-ES algorithm was run

TABLE I

OPTIMIZED PLANTARFLEXOR MORPHOLOGICAL PARAMETERS

Parameter	Initial Value	Optimal Value
F_{max}	3549 N	4000 N
l_{opt}	0.05 m	0.12 m
v_{max}	6 l_{opt}/s	5.87 l_{opt}/s
l_{slack}	0.25 m	0.08 m
r_{max}	0.06 m	0.08 m
r_{min}	0.02 m	0.08 m
ρ	0.5	0.52
w	0.56	1.90
K	5	6.05
e_{ref}	0.04	0.04

TABLE II

TUNED IMPEDANCE PARAMETER VALUES

	Stance 1	Stance 2	Swing
k (Nm/deg)	1.6	4.5	3.5
b (Nms/deg)	0.12	0.02	0.10
θ (deg)	5.0	20.0	-14.0
$t_{timeout}$ (ms)	400	500	100

for 200 iterations with 16 members per iteration to produce the torque solutions seen in Fig. 3D. The 10 plantarflexor morphological parameters and their optimal values are shown in Table I, as defined by Song *et al.* [22].

E. Controller Implementation

The TF8 powered ankle prosthesis was used to implement all controllers used in these experiments [35]. The TF8 is a sub 2.0 kg reaction force series-elastic actuator capable of biological range of sagittal motion, up to 175 Nm of peak repeated torque, and more than 400 W mechanical power at a closed-loop torque control bandwidth of 10 Hz. The mechatronics control loop is shown in Fig. 4.

The AM controller was implemented on the TF8 actuator by exporting the MATLAB Simulink *ver. R2019b (MathWorks, Inc., Natick, MA, USA)* model of the ankle with optimized plantarflexor and TA as a C++ library using the MATLAB Coder extension. The model takes as input the instantaneous prosthetic joint angle, angular velocity, and subject muscle activations to update virtual joint torque τ_{model} at a fixed rate of 1 kHz.

The output of the AM controller was calculated in parallel with the output of an impedance-based finite state machine (FSM) adapted from the work of Carney *et al.* [35]. Stance 1 was tuned to provide sufficient stabilizing impedance during heel strike and early stance. Stance 2 (Powered Plantarflexion in Carney *et al.* [35]) was tuned to provide appropriate powered plantarflexion torque for the subject. Swing was tuned to provide sufficient toe clearance after powered plantarflexion. Final tuning parameters are listed in Table II. Plantarflexion is positive angular displacement.

It is only upon entering Stance 2 that τ_{model} is set as the desired torque output τ_{des} of the actuator. In all other states, τ_{des} is set to the calculated impedance-based torque τ_{FSM}.

IV. EXPERIMENTS AND RESULTS

Because the AM paradigm should be applicable to a wide population, both stages of the cascaded optimization were preliminarily evaluated for input generalizability. For stage one, an additional digital locomotor clone was scaled to compare resultant ankle torque profiles with the test subject's clone. For stage two, synthetic plantarflexor activation trajectories were generated using a parametric distribution function to assess the bias of the agonist-antagonist controller structure.

The performance of the AM controller-prosthesis system was evaluated in three tasks: standing calf raises, treadmill walking, and level-ground walking. Affected-side prosthetic ankle angle, output torque, and muscle activity were recorded by the hardware system controller seen in Fig. 1B. Velocities of the prosthetic and unaffected ankle were derived using two-point finite differentiation of measured position. Instantaneous joint power was calculated by element-wise multiplication of velocity and torque trajectories. Net joint work was calculated as the discrete time trapezoidal integral of power. All data were recorded at 1 kHz with the exception of prosthetic ankle angle and torque, which were recorded at 800 Hz.

A. AM Paradigm Input Generalizability

The subject's clone and an additional large digital locomotor clone (1.8 m, 80 kg; from Song *et al.* [22]) were optimized to walk at 1.1 m/s. The resultant ankle torque profiles are compared to those measured from unaffected persons in Fig. 5A. A selected range of synthetic activation profiles were processed through stage two optimization to yield each one's optimal morphological parameter set according to Eq. 1. A log-normal distribution with bound support (LGNB) and variable magnitude, skewness, and kurtosis given by

$$\alpha_\sigma(t) = \frac{D(t_1-t_0)}{\sigma\sqrt{2\pi}(t-t_0)(t_1-t)} exp\left\{\frac{-1}{2\sigma^2}\left[ln\frac{(t-t_0)}{(t_1-t)}-\mu\right]^2\right\} \tag{2}$$

was used to synthesize these unimodal plantarflexor activation profiles, where D is maximum activation magnitude, t_0 the onset of support, t_1 the end of support, μ and σ^2 the mean and variance of $ln(t-t_0)$ [37]. These results are shown in Figs. 5B-D.

B. Standing Calf Raises

Bilateral standing calf raises were performed on an instrumented, split-belt treadmill while recording normal force and center of pressure of each foot. A two-axis goniometer *(Biometrics Ltd., Newport, UK)* was positioned on the subject's unaffected ankle and tared with the subject standing upright. For this experiment, the AM controller was fixed in Stance 2 to provide continuous myoelectric control. MVC for the TA was set to the 95th percentile amplitude of the observed RMS signal during a maximum contraction test with the prosthesis unpowered. To consider interactions between the subject, prosthesis, and ground, a calibration was performed to set MVC for the GAS muscle. With the prosthesis powered in Stance 2, the subject was instructed to perform repeated calf raises with the MVC of the GAS

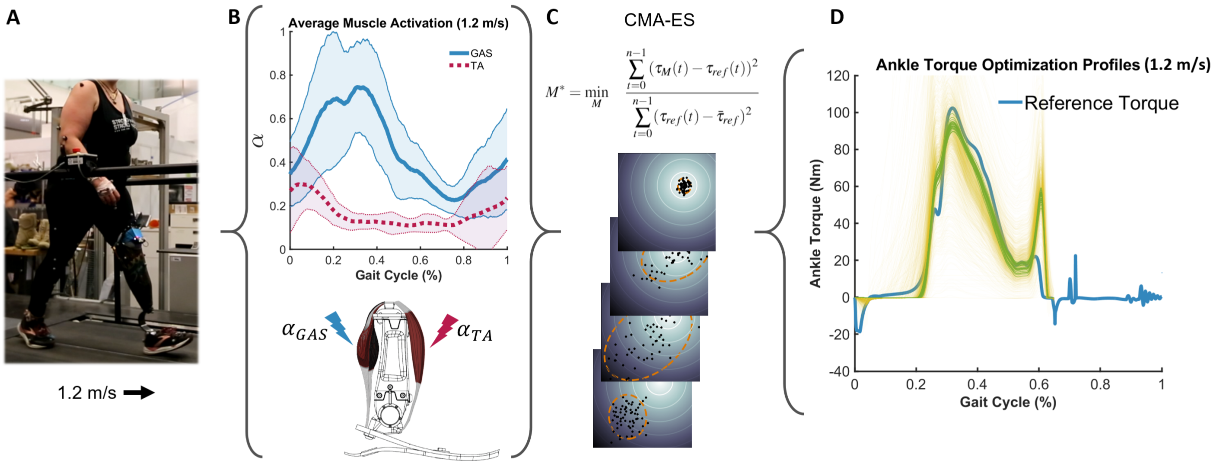

Fig. 3. Stage Two: Plantarflexor Optimization. (A) The transtibial amputee subject is asked to walk at 1.2 m/s to match the speed of the optimized digital locomotor clone. (B) Residual muscle activity is averaged and used to drive a neuromuscular ankle model kinematically-tracked to the reference ankle trajectory from stage one. (C) With these activation and kinematic trajectories, morphological parameters of the plantarflexor muscle are optimized using CMA-ES to yield (D), the optimal parameter set that best reproduces the reference torque profile obtained in stage one. Each yellow trace is torque solution, and each green trace is a torque solution with $R^2 > 0.9$.

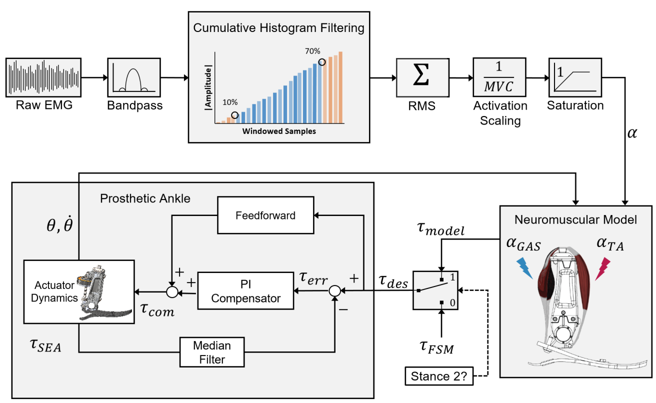

Fig. 4. Complete AM control paradigm. Raw sEMG data are processed into activations that stimulate the agonist and antagonist of the optimized neuromuscular model. The output model torque is commanded to the prosthetic actuator during the Stance 2 state of the finite state machine, corresponding to powered plantarflexion.

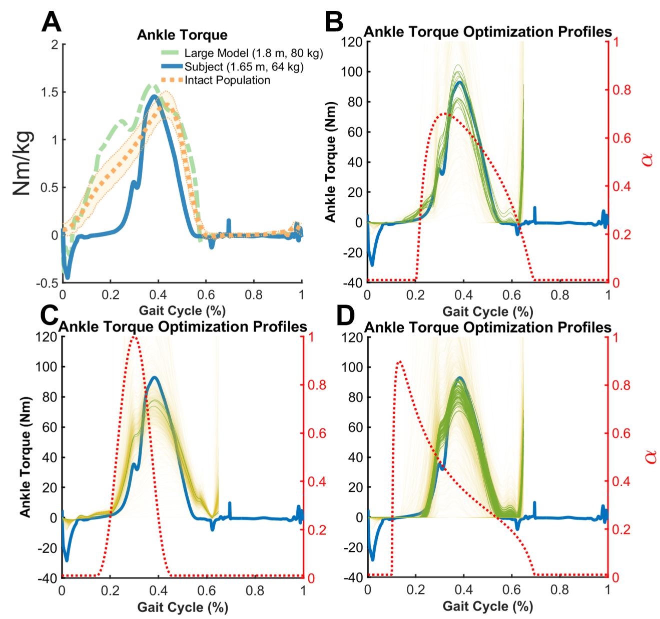

Fig. 5. Generalizability of the AM paradigm. (A) Ankle torque profiles of optimized digital locomotor clones compared to intact population $\pm 1\sigma$ at 1.1 m/s [36]. (B) Stage two optimization results with synthetic plantarflexor activation parameters $D = 0.7$, $t_0 = 0.2$, $t_1 = 0.7$, $\mu = -0.4$, $\sigma = 1.2$; (C) $D = 1$, $t_0 = 0.1$, $t_1 = 0.5$, $\mu = 0$, $\sigma = 0.6$; and (D) $D = 0.9$, $t_0 = 0.1$, $t_1 = 0.7$, $\mu = -0.9$, $\sigma = 1.5$. Green traces indicate torque solutions with $R^2 > 0.9$.

muscle initially set arbitrarily high. GAS MVC was steadily reduced until the maximum GAS activation signal calculated while the subject balanced at the maximum calf raise height observed throughout the trial peaked at 0.95. These MVCs remained unchanged for all subsequent experiments. The subject was instructed to plantarflex both prosthetic and unaffected ankles in order to balance at maximum vertical displacement for as long as possible before resting for three seconds. The subject completed three, 60 second trials, each consisting of approximately 10 calf raises. Results from this experiment are shown in Fig. 6.

C. Treadmill Walking

Treadmill walking was performed at speeds of 1.0, 1.2, and 1.4 m/s. For each speed, the subject performed a 30 second walking trial with the AM controller and a separate 30 second walking trial with the impedance-based FSM only. The subject was allowed to gently rest their hands above the safety railings, but the data associated with these sections are not reported. The subject rested for five minutes between each trial. Results from this experiment are shown in Fig. 7.

D. Level-Ground Walking

Back and forth level-ground walking was performed on a carpeted floor within a visually-marked span of 9 m. The subject completed two, 120 second level-ground walking trials using the AM controller. For each trial, the subject was

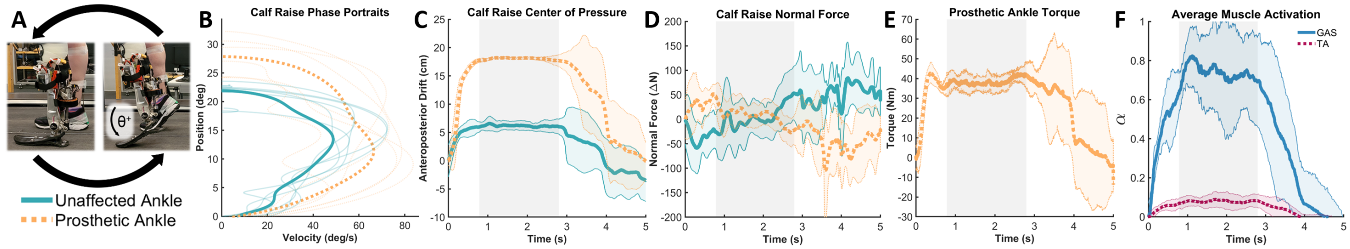

Fig. 6. Procedure diagram and aggregate results for six representative standing calf raises. Plantarflexion is represented by positive angular displacement. Mean, time-normalized trajectories are plotted in bold (shaded areas $\pm 1\sigma$). Phase portraits of individual trials are lightly plotted in subfigure B. Vertically shaded regions indicate the average period of balance, determined by the duration of both ankles within 20% of their peak angular displacement.

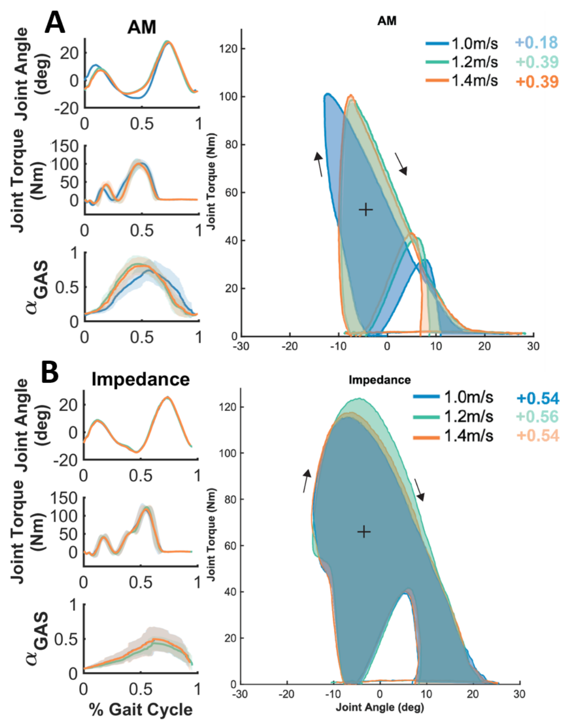

Fig. 7. Aggregate results for six consecutive prosthetic steps on a treadmill at 1.0 m/s, 1.2 m/s, and 1.4 m/s. Mean, time-normalized trajectories plotted in bold (shaded areas $\pm 1\sigma$). Shaded regions in work loops designate average positive work, and arrows indicate work loop direction. Net joint work values over one step are provided in the legend in units of Nm-rad/kg. α_{TA} never exceeded 0.2 for any trial and is omitted for brevity.

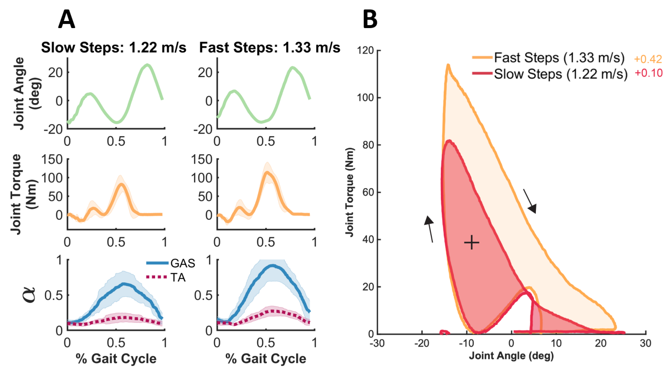

Fig. 8. Aggregate results for six consecutive prosthetic steps on level ground at self-selected slow and fast speeds using AM and impedance-based controllers. Mean, time-normalized trajectories in subfigure A are plotted in bold (shaded areas $\pm 1\sigma$). Shaded regions in subfigure B designate average positive work, and arrows indicate work loop direction. Net joint work values over one average step are provided in the legend in units of Nm-rad/kg.

instructed to walk at a speed that felt "comfortably slow" for the first half then "comfortably fast" midway through. Results from this experiment are shown in Fig. 8.

V. DISCUSSION

We present a procedural approach to designing sEMG-based prosthetic ankle controllers from a subject's objectively measured biometric data. In contrast to traditional approaches requiring hand-tuning of impedance-based parameters, the AM paradigm generates a neuromuscular controller that relies solely on the subject's input. Our resultant AM controller-prosthesis system was able to demonstrate several physiologically-relevant plantarflexion behaviors when piloted by a single subject without training.

As seen in Fig. 5A, stage one optimization was able to produce reasonable ankle torque profiles for clones of different sizes. Peak torque values are similar to those of intact humans walking at 1.1 m/s [36]. Future studies should investigate if the deviations in early stance torque are attributable to unique subject-specific traits or modeling error. Stage two optimization was also able to find accurate solutions for a variety of input plantarflexor activations, as seen in Fig. 5B-D. These results present the possibility of effective application of the AM paradigm to a more diverse amputee population in future studies.

The calf raise experiment is performed in bilateral symmetry, requiring coordination between unaffected and prosthetic ankle joints. It is understood that volitional coordination of an unaffected joint with a prosthetic joint controlled by amputated musculature will demonstrate similar velocity profiles when well-coordinated [38]. The average phase portraits of both joints can be seen in Fig. 6B to agree in shape, if not in magnitude of angular displacement at apex. The angular difference can be explained by the noticeably shorter prosthetic foot seen in Fig. 6A, meaning that for a given vertical body displacement, the prosthetic ankle must plantarflex to a greater degree than the unaffected ankle. The notion that both ankles displace the same distance vertically at apex is supported by Fig. 6D, which shows that body weight is evenly distributed during the shaded portion when the subject is balanced on tiptoe. The center of pressure for the prosthetic foot is noticeably anterior to that of the unaffected foot in Fig. 6C, though this is explained by the difference in contact patch size stemming from the prosthetic foot's lack of metatarsal-phalangeal joint. Overall, prosthetic ankle torque and average muscle activation were observed to hold steady at apex, as shown in Figs. 6E and F, which likely contributed to the subject's ability to maintain a balanced posture for an average of 2.13 seconds.

Results from treadmill walking suggest invariance of prosthetic ankle dynamics produced by impedance control at tested speeds, as seen in Fig. 7B. Generated ankle torque profiles and work loops, while within physiological ranges, do not demonstrate typical indicators of speed adaptation, such as hastened time of peak torque, increased maximum plantarflexion angle, increased peak torque, and increased net work [39]. However, by these metrics, neither do dynamics generated under AM control completely agree with literature. Comparing 1.0 m/s and 1.4 m/s trajectories in Fig. 7A, time of peak torque was hastened and net work was increased, but peak torque and maximum plantarflexion angle remained largely static. While an invariant maximum plantarflexion angle may potentially be attributed to the fact that transitioning from Stance 2 to Swing is identical between both controllers, additional testing is required to confidently attribute sources of error. Notably, while GAS activation patterns remain delayed and physiologically irrelevant at all tested speeds under impedance control, GAS activation patterns under AM control demonstrate both hastened peak time and increased peak magnitude, suggesting that the subject is capable of generating sufficient information to demonstrate typical indicators of speed adaption.

Level-ground walking under AM control clearly produced indicators of speed adaption, as seen in Fig. 8 by the hastened peak torque, increased peak torque, and drastically increased net work from 1.22 m/s to 1.33 m/s. GAS activation is also observed to qualitatively correlate with these changes. Differences in performance compared to treadmill walking may pertain to optical flow [40]. Alternatively, or additionally, it has been found that while kinematic patterns between treadmill and level-ground walking are largely similar, muscle activations and developed joint torques may differ significantly [41]. A population study would be more appropriate for identifying any significant differences between the two walking modes under AM control.

Although muscle reflexes are essential for physiological gait, amputation musculature cannot provide instantaneous kinesthetic feedback from ground reaction forces. The AM paradigm compensates by converging onto a controller that translates user-generated sEMG, whatever its profile, to gait-restoring ankle torque. However, other feedback signals containing cutaneous and pressure information may still facilitate reflexive within-step adjustments. Additionally, vestibular and optical sensory information from the central nervous system may enable step-by-step feedforward modulation of muscle activation, similar to Huang *et al.*'s ballistic control paradigm [42], whereby the subject assesses their previous discrete repetition to prepare for the subsequent. The actual contribution of the AM paradigm in accounting for these factors should be reassessed in future work through comparison with a simpler controller that generates torque proportional to sEMG, in a manner similar to Huang *et al.* [16].

This study simplified the dynamics, geometry, and inertia of the powered prosthetic ankle to be identical to the digital locomotor clone's ankle, resulting in idealized, symmetric walking dynamics. However, a study by Handford and Srinivasan suggests optimal gait may deviate from bilateral symmetry when considering actual prosthesis dynamics [43]. Another assumption made for stage two optimization was the invariance of within-socket sEMG generated between passive prosthetic ankle and powered prosthetic ankle, an assumption shown to be untrue, as seen in Fig. 3B and Fig. 7B. Finally, this pilot study collected data from an individual with the AMI amputation. From other studies comparing AMI and non-AMI subjects, it is likely that performance between the populations under the AM controller paradigm would differ significantly [17][38]. Overall, additional consideration is required before further generalizing the AM controller.

VI. Conclusion

In this letter, we explain an approach to neuroprosthetic controller design that prioritizes objective measurements of the amputee subject over subjective judgments. Because the powered prosthetic device is constrained to one degree of freedom, and the AMI is a reduced-dimension analog for the lower extremities with no muscular redundancy, our approach necessarily reduces the complexities of gait and muscle dynamics into a tractable form with each optimization stage. Despite these simplifications, we demonstrated the emergence of bilaterally symmetric coordination and speed adaptation over level ground in an untethered, volitionally-controlled neuroprosthesis.

References

[1] K. E. Zelik, K. Z. Takahashi, and G. S. Sawicki, "Six degree-of-freedom analysis of hip, knee, ankle and foot provides updated understanding of biomechanical work during human walking," *Journal of Experimental Biology*, vol. 218, no. 6, pp. 876–886, 2015. [Online]. Available: https://jeb.biologists.org/content/218/6/876

[2] J. R. Usherwood, A. J. Channon, J. P. Myatt, J. W. Rankin, and T. Y. Hubel, "The human foot and heel-sole-toe walking strategy: a mechanism enabling an inverted pendular gait with low isometric muscle force?" *Journal of The Royal Society Interface*, vol. 9, no. 75, pp. 2396–2402, 2012. [Online]. Available: https://royalsocietypublishing.org/doi/abs/10.1098/rsif.2012.0179

[3] S. Collins, A. Ruina, R. Tedrake, and M. Wisse, "Efficient bipedal robots based on passive-dynamic walkers," *Science*, vol. 307, no. 5712, pp. 1082–1085, 2005. [Online]. Available: https://science.sciencemag.org/content/307/5712/1082

[4] S. W. Lipfert, M. Günther, D. Renjewski, and A. Seyfarth, "Impulsive ankle push-off powers leg swing in human walking," *Journal of Experimental Biology*, vol. 217, no. 8, pp. 1218–1228, 2014. [Online]. Available: https://jeb.biologists.org/content/217/8/1218

[5] H. Houdijk, E. Pollmann, M. Groenewold, H. Wiggerts, and W. Polomski, "The energy cost for the step-to-step transition in amputee walking," *Gait & Posture*, vol. 30, no. 1, pp. 35 – 40, 2009. [Online]. Available: http://www.sciencedirect.com/science/article/pii/S0966636209000642

[6] H. M. Herr and A. M. Grabowski, “Bionic ankle & foot prosthesis normalizes walking gait for persons with leg amputation,” *Proceedings of the Royal Society B: Biological Sciences*, vol. 279, no. 1728, pp. 457–464, 2012. [Online]. Available: https://royalsocietypublishing.org/doi/abs/10.1098/rspb.2011.1194

[7] C. H. Lloyd, S. J. Stanhope, I. S. Davis, and T. D. Royer, “Strength asymmetry and osteoarthritis risk factors in unilateral trans-tibial, amputee gait,” *Gait & Posture*, vol. 32, no. 3, pp. 296 – 300, 2010. [Online]. Available: http://www.sciencedirect.com/science/article/pii/S096663621000127X

[8] P. Cherelle, G. Mathijssen, Q. Wang, B. Vanderborght, and D. Lefeber, “Advances in propulsive bionic feet and their actuation principles,” *Advances in Mechanical Engineering*, vol. 2014, 2014, cited By 26.

[9] M. Tschiedel, M. F. Russold, and E. Kaniusas, “Relying on more sense for enhancing lower limb prostheses control: a review,” *J. NeuroEng. Rehabil.*, vol. 17, no. 1, pp. 1–13, Dec 2020.

[10] M. R. Tucker, J. Olivier, A. Pagel, H. Bleuler, M. Bouri, O. Lambercy, J. del R. Millán, R. Riener, H. Vallery, and R. Gassert, “Control strategies for active lower extremity prosthetics and orthotics: a review,” *J. NeuroEng. Rehabil.*, vol. 12, no. 1, pp. 1–30, Dec 2015.

[11] S. K. Au, P. Bonato, and H. Herr, “An emg-position controlled system for an active ankle-foot prosthesis: an initial experimental study,” in *9th International Conference on Rehabilitation Robotics, 2005. ICORR 2005.*, 2005, pp. 375–379.

[12] S. Au, M. Berniker, and H. Herr, “Powered ankle-foot prosthesis to assist level-ground and stair-descent gaits,” *Neural Networks*, vol. 21, no. 4, pp. 654–666, May 2008.

[13] J. Wang, O. A. Kannape, and H. M. Herr, “Proportional emg control of ankle plantar flexion in a powered transtibial prosthesis,” in *2013 IEEE 13th International Conference on Rehabilitation Robotics (ICORR)*, 2013, pp. 1–5.

[14] D. P. Ferris, K. E. Gordon, G. S. Sawicki, and A. Peethambaran, “An improved powered ankle-foot orthosis using proportional myoelectric control,” *Gait & Posture*, vol. 23, no. 4, pp. 425–428, Jun 2006.

[15] S. M. Cain, K. E. Gordon, and D. P. Ferris, “Locomotor adaptation to a powered ankle-foot orthosis depends on control method,” *J. NeuroEng. Rehabil.*, vol. 4, no. 1, pp. 1–13, Dec 2007.

[16] S. Huang, J. P. Wensman, and D. P. Ferris, “Locomotor adaptation by transtibial amputees walking with an experimental powered prosthesis under continuous myoelectric control,” *IEEE Transactions on Neural Systems and Rehabilitation Engineering*, vol. 24, no. 5, pp. 573–581, 2016.

[17] T. R. Clites, M. J. Carty, J. B. Ullauri, M. E. Carney, L. M. Mooney, J.-F. Duval, S. S. Srinivasan, and Hugh. M. Herr, “Proprioception from a neurally controlled lower-extremity prosthesis,” *Science Translational Medicine*, vol. 10, no. 443, May 2018.

[18] G. M. Hefferman, F. Zhang, M. J. Nunnery, and H. Huang, “Integration of surface electromyographic sensors with the transfemoral amputee socket: A comparison of four differing configurations,” *Prosthetics and orthotics international*, vol. 39, no. 2, pp. 166–173, 2015.

[19] S. H. Yeon, T. Shu, E. A. Rogers, H. Song, T. H. Hsieh, L. E. Freed, and H. M. Herr, “Flexible dry electrodes for emg acquisition within lower extremity prosthetic sockets,” in *2020 8th IEEE RAS/EMBS International Conference for Biomedical Robotics and Biomechatronics (BioRob)*, 2020, pp. 1088–1095.

[20] S. H. Yeon, T. Shu, H. Song, T.-H. Hsieh, J. Qiao, E. A. Rogers, S. Gutierrez-Arango, E. Israel, L. E. Freed, and H. M. Herr, “Acquisition of surface emg using flexible and low-profile electrodes for lower extremity neuroprosthetic control,” *IEEE Transactions on Medical Robotics and Bionics*, vol. 3, no. 3, pp. 563–572, 2021.

[21] H. Geyer and H. Herr, “A Muscle-Reflex Model That Encodes Principles of Legged Mechanics Produces Human Walking Dynamics and Muscle Activities,” *IEEE Transactions on Neural Systems and Rehabilitation Engineering*, vol. 18, no. 3, pp. 263–273, Apr 2010.

[22] S. Song and H. Geyer, “A neural circuitry that emphasizes spinal feedback generates diverse behaviours of human locomotion,” *The Journal of Physiology*, vol. 593, no. 16, pp. 3493–3511, 2015. [Online]. Available: https://physoc.onlinelibrary.wiley.com/doi/abs/10.1113/JP270228

[23] N. Hansen and A. Ostermeier, “Adapting arbitrary normal mutation distributions in evolution strategies: the covariance matrix adaptation,” in *Proceedings of IEEE International Conference on Evolutionary Computation*. IEEE, May 1996, pp. 312–317.

[24] M. F. Eilenberg, H. Geyer, and H. Herr, “Control of a powered ankle–foot prosthesis based on a neuromuscular model,” *IEEE Transactions on Neural Systems and Rehabilitation Engineering*, vol. 18, no. 2, pp. 164–173, 2010.

[25] J. Markowitz, P. Krishnaswamy, M. F. Eilenberg, K. Endo, C. Barnhart, and H. Herr, “Speed adaptation in a powered transtibial prosthesis controlled with a neuromuscular model,” *Philosophical Transactions of the Royal Society B: Biological Sciences*, vol. 366, no. 1570, p. 1621, May 2011.

[26] J. Zhao, K. Berns, R. de Souza Baptista, and A. P. L. Bó, “Design of variable-damping control for prosthetic knee based on a simulated biped,” in *2013 IEEE 13th International Conference on Rehabilitation Robotics (ICORR)*. IEEE, June 2013, pp. 1–6.

[27] T. R. Clites, H. M. Herr, S. S. Srinivasan, A. N. Zorzos, and M. J. Carty, “The ewing amputation: The first human implementation of the agonist-antagonist myoneural interface,” *Plastic and Reconstructive Surgery Global Open*, vol. 6, no. 11, Nov 2018.

[28] S. H. Yeon, “Design of an advanced semg processor for wearable robotics applications,” Master’s thesis, Massachusetts Institute of Technology, 2019.

[29] C. J. De Luca, “The use of surface electromyography in biomechanics,” *Journal of applied biomechanics*, vol. 13, no. 2, pp. 135–163, 1997.

[30] C. J. De Luca, L. D. Gilmore, M. Kuznetsov, and S. H. Roy, “Filtering the surface emg signal: Movement artifact and baseline noise contamination,” *Journal of biomechanics*, vol. 43, no. 8, pp. 1573–1579, 2010.

[31] S. H. Yeon and H. M. Herr, “Rejecting impulse artifacts from surface emg signals using real-time cumulative histogram filtering,” in *2021 43rd Annual International Conference of the IEEE Engineering in Medicine & Biology Society (EMBC)*. IEEE, 2021, pp. 6235–6241.

[32] W. T. Dempster and G. R. Gaughran, “Properties of body segments based on size and weight,” *American Journal of Anatomy*, vol. 120, no. 1, January 1967.

[33] S. Delp, F. C. Anderson, A. S. Arnold, P. Loan, A. Habib, C. T. John, E. Guendelman, and D. G. Thelen, “Opensim: Open-source software to create and analyze dynamic simulations of movement,” *IEEE Transactions on Biomedical Engineering*, vol. 54, no. 11, 2007.

[34] A. Seth, J. L. Hicks, T. K. Uchida, A. Habib, C. L. Dembia, J. J. Dunne, C. F. Ong, M. S. DeMers, A. Rajagopal, M. Millard, S. R. Hamner, E. M. Arnold, J. R. Yong, S. K. Lakshmikanth, M. A. Sherman, J. P. Ku, and S. L. Delp, “Opensim: Simulating musculoskeletal dynamics and neuromuscular control to study human and animal movement,” *PLoS Computational Biology*, vol. 14, no. 7, 2018.

[35] M. E. Carney, T. Shu, R. Stolyarov, J.-F. Duval, and H. M. Herr, “Design and preliminary results of a reaction force series elastic actuator for bionic knee and ankle prostheses,” *IEEE Transactions on Medical Robotics and Bionics*, vol. 3, no. 3, pp. 542–553, 2021.

[36] S. Lipfert, *Kinematic and dynamic similarities between walking and running*, 01 2010.

[37] R. Plamondon, A. M. Alimi, P. Yergeau, and F. Leclerc, “Modelling velocity profiles of rapid movements: a comparative study,” *Biol. Cybern.*, vol. 69, no. 2, pp. 119–128, Jun 1993.

[38] T. Shu, S. S. Huang, C. Shallal, and H. M. Herr, “Restoration of bilateral motor coordination from preserved agonist-antagonist coupling in amputation musculature,” *Journal of NeuroEngineering and Rehabilitation*, vol. 18, no. 1, pp. 1–17, Dec 2021.

[39] M. Grimmer and A. Seyfarth, “Mimicking Human-Like Leg Function in Prosthetic Limbs,” in *Neuro-Robotics: From Brain Machine Interfaces to Rehabilitation Robotics*. Dordrecht, The Netherlands: Springer, Jun 2014, pp. 105–155.

[40] W. H. Warren, B. A. Kay, W. D. Zosh, A. P. Duchon, and S. Sahuc, “Optic flow is used to control human walking - Nature Neuroscience,” *Nature Neuroscience*, vol. 4, no. 2, pp. 213–216, Feb 2001.

[41] S. J. Lee and J. Hidler, “Biomechanics of overground vs. treadmill walking in healthy individuals,” *Journal of Applied Physiology*, Mar 2008. [Online]. Available: https://journals.physiology.org/doi/full/10.1152/japplphysiol.01380.2006

[42] S. Huang and H. Huang, “Voluntary Control of Residual Antagonistic Muscles in Transtibial Amputees: Feedforward Ballistic Contractions and Implications for Direct Neural Control of Powered Lower Limb Prostheses,” *IEEE Trans. Neural Syst. Rehabil. Eng.*, vol. 26, no. 4, pp. 894–903, Mar. 2018.

[43] M. L. Handford and M. Srinivasan, “Energy-Optimal Human Walking With Feedback-Controlled Robotic Prostheses: A Computational Study,” *IEEE Transactions on Neural Systems and Rehabilitation Engineering*, vol. 26, no. 9, pp. 1773–1782, Jul 2018.